Imidodiphosphonate Ligands for Enhanced Sensitization and Shielding of Visible and Near-Infrared Lanthanides

Dita Davis,[†,#] Andrew J. Carrod,[†,#] Zhilin Guo,[†,‡] Benson M. Kariuki,[§] Yuan-Zhu Zhang,[‡] and Zoe Pikramenou*[,†]

[†]School of Chemistry, The University of Birmingham, Edgbaston B15 2TT, United Kingdom

[‡]Department of Chemistry, Southern University of Science and Technology, Shenzhen 518055, China [§]School of Chemistry, Cardiff University, Cardiff CF10 3AT, United Kingdom

* Supporting Information

ABSTRACT: The design of coordination sites around lanthanide ions has a strong impact on the sensitization of their luminescent signal. An imidodiphosphonate anionic binding site is attractive as it can be functionalized with "remote" sensitizer units, such as phenoxy moieties, namely, HtpOp, accompanied by an increased distance of the lanthanide from the ligand high-energy stretching vibrations which quench the luminescence signal, hence providing flexible shielding of the lanthanide. We report the formation and isolation of $Ln(tpOp)_3$ complexes where Ln = Er, Gd, Tb, Dy, Eu, and Yb and the $Y(tpOp)_3$ diamagnetic analogue. The complexes are formed from reaction of KtpOp and the corresponding $LnCl_3{\cdot}6H_2O$ salt either by titration and in situ formation or by mixing and isolation. All complexes are seven-coordinated by three tpOp ligand plus one ethanol molecule, except for $Yb(tpOp)_3$ which has no solvent coordinated. Phosphorus NMR shows characteristic shifts to support the coordination of the lanthanide complexes. The complexes display visible and near-infrared luminescence with long lifetimes even for the near-infrared complexes which range from 3.3 μs for $Nd(tpOp)_3$ to 20 μs for $Yb(tpOp)_3$. The ligand shows more efficient sensitization than the imidodiphosphinate analogues for all lanthanide complexes with a notable quantum yield of the $Tb(tpOp)_3$ complex at 45%. We attribute this to the properties of the remote sensitizer unit and its positioning further away from the lanthanide, eliminating quenching of high energy C−H vibrations from the ligand shell. Calculations of the ligand shielding support the photophysical properties of the complexes. These results suggest that these binding sites are promising in the further development of the lanthanide complexes in optoelectronic devices for telecommunications and new light emitting materials.

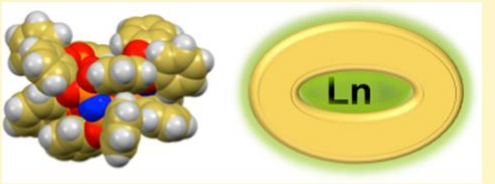

INTRODUCTION

Lanthanide coordination complexes are popular luminescent probes offering a range of signal detection from the visible to the near-infrared[1,2] region with characteristic long-lived lifetimes important for their incorporation in optoelectronic devices for sensing and telecommunications.[3−5] Their luminescent output is controlled by the efficiency of the sensitization process from the ligand and the reduction of nonradiative quenching pathways mainly from high-energy vibrations in the proximity of the lanthanide coordination site and the presence of charge transfer bands (most relevant for Eu^{3+} and Yb^{3+} complexes).[1] The ligand design is also limited by the triplet state energy level of the sensitizer which is responsible for energy transfer to the lanthanide, providing a challenge for a single ligand to sensitize efficiently all lanthanides.[6] We have previously shown that imidodiphosphinate ligands provide a bidentate binding site to coordinate to the lanthanide forming a six-membered ring with the lanthanide and providing a "remote to the metal center" sensitizing unit.[7−10] The tetraphenyl imidodiphosphinate ligand (Htpip) forms a hydrophobic shell around the lanthanide ions stabilizing a six-coordinate complex.[7,8] The interesting feature of this design is that the ligands provide twelve sensitizers around one lanthanide, which can be modified independently of the binding site. Modification of the ligand shell with fluorinated phenyl groups to exclude all C−H high energy vibrations demonstrated long lifetimes in the near-infrared region and such complexes have been studied in devices as a promising optical amplifier material.[4,10,11]

We have been interested in the influence of increased polarity and extension of the shell around the lanthanide when a more flexible shell is introduced. We chose the tetraphenyl imidodiphosphonate, HtpOp, which positions the sensitizer group further from the lanthanide but provides a more flexible extended "shell" around the lanthanide to study the effect on the lanthanide luminescence signal and establish the imidophosphonate group as a new sensitizer for the lanthanides (Scheme 1). The substitution of phenyl groups for phenoxide was sought to also increase the solubility of the metal complex in polar solvents. The X-ray crystal structure of the ligand has been previously reported,[12−14] and the

Scheme 1. Structures of HtpOp and Htpip

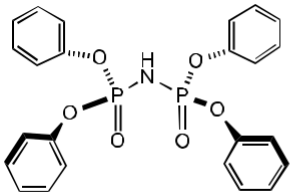

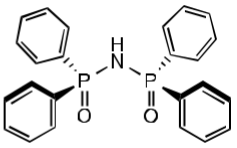

formation of the lanthanide complexes has been mentioned with only elemental analysis reported,[15] apart from the ytterbium crystal structure.[16,17]

We report herein the synthesis and full characterization of all the lanthanide complexes Ln(tpOp)$_3$ (Ln = Eu, Tb, Dy, Sm, Gd, Er, Nd, and Yb) prepared from a key intermediate KtpOp, as well as the formation of Y(tpOp)$_3$ as a diamagnetic analogue. A detailed analysis of their photophysical properties based on their luminescence lifetimes and quantum yields is reported to evaluate the complexes for their potential applications in optical materials.

EXPERIMENTAL SECTION

General Methods. All the chemicals and solvents were commercially available from Sigma-Aldrich, Alfa Aesar or Fisher Scientific. NMR spectra were obtained on Bruker AC 300, AV 300, AMX 400, AV 400, or DRX 500 spectrometers. Electrospray mass spectra were recorded on a Micromass LC-TOF machine. Elemental analyses were recorded on a Carlo Erba EA1110 simultaneous CHN elemental analyzer. Single-crystal diffraction data were recorded on a Bruker Smart 6000 diffractometer equipped with a CCD detector and a copper tube source. The structures were solved by direct methods and refined with the SHELXT.[18] Generally, restraints were applied to the geometry and atomic displacement parameters where disorder occurred. Except for water molecules, hydrogen atom geometry was idealized and they were refined using a riding model. The ligand shielding was calculated using the program Solid-G.[19]

Photophysical Studies. UV−vis absorption spectra were recorded on an Agilent Cary 60 UV−vis spectrophotometer. Luminescence spectra were recorded on an Edinburgh Instruments FLSP920 steady-state and time-resolved spectrometer with F900 software and on a Photon Technology International spectrometer. The excitation and emission spectra are corrected for lamp/ photomultiplier tube/instrument response as required according to spectral response correction files recommended by the manufacturer. Time-resolved lifetime measurements were carried out by using a Continuum Surelight Nd:YAG laser (10 Hz, 4−6 ns) as the excitation source using a 355 nm harmonic. Data were recorded using a LeCroy 9350AM 500 MHz oscilloscope. Lifetimes were fitted with Kaleida-Graph software using a nonlinear least-squares iterative technique. The luminescence quantum yields for Tb(tpOp)$_3$, Eu(tpOp)$_3$, Dy(tpOp)$_3$, Nd(tpOp)$_3$, and Yb(tpOp)$_3$ were measured with an integrating sphere apparatus from Edinburgh Instruments. In the quantum yield measurements, we used standards to validate the instrumental set up as recommended in the IUPAC technical reports.[20,21] Each sample was measured several times under comparable conditions. The quantum yield for Sm(tpOp)$_3$ was determined using the optical dilute method with [Ru(bpy)$_3$]Cl$_2$ as the reference.[22]

Synthesis of HtpOp. A suspension of triphenyl phosphate (6.01 g, 18.4 mmol) and sodium amide (1.51 g, 8.59 mmol) in 60 mL of dry toluene was heated at reflux for 4 h under N_2. The resulting mixture was cooled to 40 °C, and 50 mL of water was added to dissolve the sodium phenoxide. The toluene layer was extracted, acidified with dilute HCl (9.2 mL, 1 M), and washed with water (2 × 20 mL). The volume of the solution was concentrated to about 4 mL, and 40 mL of hexane was added. The solution was then stirred until a white precipitate was formed. The desired white product (2.73 g, 62%) was collected by filtration, washed with hexane (2 × 10 mL) and dried under vacuum. Mp = 109 °C. δP{^{1}H} (121 MHz, CDCl$_3$): −10.5 (s). δC{^{1}H} (75 MHz, CDCl$_3$): 150.6 (C1), 130.1 (C3) 125.9 (C4), 120.9 (C2). δH (300 MHz, CDCl$_3$): 7.11−7.24 (20H, m, Ar). MS (ES$^-$) m/z: 480 [M − H]$^-$. Elemental analysis calcd (%) for $C_{24}H_{21}NO_6P_2$: C, 59.88; H, 4.40; N, 2.91. Found: C, 59.61; H, 4.20; N 2.98. UV/vis (CH$_3$CN): λ in nm (log ε) 263 (3.2). IR: ν_{max}/cm^{-1} 2961 (m, br, N−H), 2753 (m, br, C−H), 1800−2100 (w, br, C C), 1184 (s, P O), 933 (s, P−N−P).

Synthesis of KtpOp. Potassium hydride (0.49 g, 35% dispersion in mineral oil, 3.69 mmol) was washed with pentane (3 × 5 mL) under N_2 and dried in vacuo for 20 min. THF (8 mL) was then added, followed by HtpOp (1.54 g, 3.20 mmol) dissolved in 15 mL of THF. The resulting suspension was stirred for 1 h at room temperature under N_2. The solvent was removed in vacuo to yield a light brown viscous solution, which was dissolved in water (8 mL) and extracted with pentane (3 × 5 mL). The volume of the aqueous layer was reduced in vacuo, and the residue was transferred to the freezer overnight. The resulting light brown solid was washed with pentane (5 × 10 mL) and dried under vacuum to yield the desired product (1.46 g, 88%). δP{^{1}H} (121 MHz, CDCl$_3$): −7.2 (s). δC{^{1}H} (75 MHz, CDCl$_3$): 155.1(C1), 132.0 (C3) 126.6 (C4), 123.3 (C2). δH (300 MHz, CDCl$_3$): 6.94−7.11 (20H, m, Ar). MALDI-MS m/z: 519.6 [M]$^+$, 557.6 [M + K]$^+$. Elemental analysis calcd (%) for $C_{24}H_{20}NO_6P_2K(H_2O)$: C, 53.63; H, 4.13; N, 2.61. Found: C, 53.64; H, 3.67; N 2.70. Exact mass m/z (ESI-TOF) $C_{24}H_{21}NO_6P_2K$ calcd: 520.0481. Found: 520.0484.

Synthesis of Ln(tpOp)$_3$ (Ln = Eu, Tb, Dy, Sm, Gd, Nd, Er, and Yb) and Y(tpOp)$_3$. To a stirring solution of KtpOp (0.39 mmol) in EtOH (10 mL) a solution of LnCl$_3$·6H$_2$O (0.13 mmol) in EtOH (5 mL) was added dropwise. The resulting white suspension was then stored at −18 °C overnight, yielding a white, sticky precipitate. The solvent was decanted off, and the remaining solid was stirred vigorously with hexane (5 mL) to yield the product as a fine white powder. The powder was collected by filtration, washed with hexane (2 × 5 mL), and dried under vacuum.

Eu(tpOp)$_3$. Yield: 0.13 g, 63%. δP{^{1}H} (121 MHz, CDCl$_3$): −80.0 (s). δC{^{1}H} (75 MHz, CDCl$_3$): 148.5 (C1), 128.0 (C3), 123.0 (C4), 119.2 (C2). δH (300 MHz, CDCl$_3$): 7.29 (24H, t, $^3J_{(H,H)}$ = 7.3 Hz, Hb), 7.19 (12H, t, $^3J_{(H,H)}$ = 7.1 Hz, Hc), 6.78 (24H, d, $^3J_{(H,H)}$ = 7.6 Hz, Ha). MS (ESI$^+$): m/z 1616 [M + Na]$^+$. Elemental analysis calcd (%) for $C_{72}H_{60}N_3O_{18}P_6Eu$: C, 54.28; H, 3.80; N, 2.64. Found: C, 54.14; H, 3.98; N 2.82. UV/vis (CH$_3$CN): λ in nm (log ε) 263 (3.7).

Tb(tpOp)$_3$. Yield: 0.12 g, 59%. δP{^{1}H} (121 MHz, CDCl$_3$): −33.8 (br,s). δC{^{1}H} (75 MHz, CDCl$_3$): 163.9 (C1), 126.2 (C3), 123.2 (C2), 121.2 (C4). δH (300 MHz, CDCl$_3$): 6.35 (24H, br, Ha), 4.01 (12H, s, Hc), 3.21 (24H, s, Hb). MS (ESI$^+$): m/z 1638 [M + K]$^+$. Elemental analysis calcd (%) for $C_{72}H_{60}N_3O_{18}P_6Tb$: C, 54.05; H, 3.78; N, 2.63. Found: C, 53.83; H, 4.02; N 2.79. UV/vis (CH$_3$CN): λ in nm (log ε) 263 (3.7).

Dy(tpOp)$_3$. Yield: 0.12 g, 58%. δP{^{1}H} (121 MHz, CDCl$_3$): −2.2 (br,s). δC{1H} (75 MHz, CDCl$_3$): 163.0 (C1), 128.2 (C3), 123.5 (C2), 120.5 (C4). δH (300 MHz, CDCl$_3$): 5.66 (24H, br, Ha), 4.25 (12H, s, Hc), 3.32 (24H, s, Hb). MS (ESI$^+$): m/z 1643 [M + K]+. Elemental analysis calcd (%) for $C_{72}H_{60}N_3O_{18}P_6Dy$: C, 53.93; H, 3.77; N, 2.62. Found: C, 54.10; H, 3.63; N 2.67. UV/vis (CH$_3$CN): λ in nm (log ε) 263 (3.7). IR: ν_{max}/cm^{-1} 1900 2100 (w, C C), 1150 (s, P O), 921 (m, P−N−P).

Sm(tpOp)$_3$. Yield: 0.11 g, 52%. δP{1H} (121 MHz, CDCl$_3$): −4.0 (s). δC{1H} (75 MHz, CDCl$_3$): 151.5 (C1), 129.2 (C3), 124.2 (C4), 120.8 (C2). δH (300 MHz, CDCl$_3$): 7.13 (24H, d, $^3J_{(H,H)}$ = 7.9 Hz, Ha), 7.02 (24H, t, $^3J_{(H,H)}$ = 7.5 Hz, Hb), 6.93 (12H, t, $^3J_{(H,H)}$ = 6.9 Hz, Hc). MALDI-MS: m/z 1591.5 [M]$^+$. Elemental analysis calcd (%) for $C_{72}H_{60}N_3O_{18}P_6Sm$: C, 54.34; H, 3.80; N, 2.64. Found: C, 54.15; H, 3.92; N 2.67. UV/vis (CH$_3$CN): λ in nm (log ε) 263 (3.7).

Gd(tpOp)$_3$. Yield: 0.13 g, 58%. MS (ESI$^+$): m/z 1637 [M + K]$^+$. Elemental analysis calcd (%) for $C_{72}H_{60}N_3O_{18}P_6Gd$: C, 54.10; H, 3.78; N, 2.63. Found: C, 54.10; H, 3.94; N 2.66. UV/vis (CH$_3$CN): λ in nm (log ε) 263 (3.6).

Nd(tpOp)$_3$. Yield: 0.11 g, 56%. δP{^{1}H} (121 MHz, $CDCl_3$): 30.2. δC{^{1}H} (75 MHz, $CDCl_3$): 155.7 (C1), 131.6 (C3), 126.5 (C4), 123.4 (C2). δH (300 MHz, $CDCl_3$): 6.73−6.80 (60H, m, Ar). MS (ESI^+): m/z 1623 $[M + K]^+$. Elemental analysis calcd (%) for $C_{72}H_{60}N_3O_{18}P_6Nd$: C, 54.55; H, 3.81; N, 2.65. Found: C, 54.25; H, 3.63; N 2.77. UV/vis (CH_3CN): λ in nm (log ε) 263 (3.7).

Er(tpOp)$_3$. Yield: 0.14 g, 67%. δP{1H} (121 MHz, $CDCl_3$): −85.8. δC{1H} (75 MHz, $CDCl_3$): 147.2 (C1), 128.4 (C3), 123.5 (C4), 119.5 (C2). δH (300 MHz, $CDCl_3$): 8.16 (24H, br, s, Ha), 7.76 (24H, br, s, Hb), 7.38 (12H, br, s, Hc). MS (ESI^+): m/z 1647 $[M + K]^+$. Elemental analysis calcd (%) for $C_{72}H_{60}N_3O_{18}P_6Er$: C, 53.78; H, 3.81; N, 2.61. Found: C, 53.70; H, 3.81; N 3.02. UV/vis (CH_3CN): λ in nm (log ε) 263 (3.6).

Yb(tpOp)$_3$. Yield: 0.13 g, 65%. δP{^{1}H} (121 MHz, $CDCl_3$): −8.5 (s). δC{^{1}H} (75 MHz, $CDCl_3$): 147.7 (C1), 128.5 (C3), 123.6 (C4), 119.5 (C2). δH (300 MHz, $CDCl_3$): 8.59 (24H, br, s, Ha), 7.81 (24H, br, s, Hb), 7.38 (12H, t, $^3J_{(H,H)}$ = 7.3 Hz, Hc). MS (ESI^+): m/z 1653 $[M + K]^+$. Elemental analysis calcd (%) for $C_{72}H_{60}N_3O_{18}P_6Yb$: C, 53.58; H, 3.75; N, 2.60. Found: C, 53.59; H, 3.74, N, 2.59. UV/vis (CH_3CN): λ in nm (log ε) 263 (3.6).

Y(tpOp)$_3$. Yield: 0.13 g, 66%. δP{^{1}H} (121 MHz, $CDCl_3$): −4.2. δC{^{1}H} (75 MHz, $CDCl_3$): 150.7 (C1), 128.8 (C3), 123.9 (C4), 120.2 (C2). δH (300 MHz, $CDCl_3$): 6.93−7.05 (60H, m, Ar). MS (ESI^+): m/z 1569 $[M + K]^+$. Elemental analysis calcd (%) for $C_{72}H_{60}N_3O_{18}P_6Y$: C, 56.52; H, 3.95; N, 2.75. Found: C, 56.71; H, 3.94; N, 2.73. UV/vis (CH_3CN): λ in nm (log ε) 263 (3.6).

RESULTS AND DISCUSSION

Synthesis and Characterizations of HtpOp and KtpOp. We report herein the full characterization of the HtpOp ligand (Scheme 1) prepared with a modification of a previously reported method,[12] and the preparation of the KtpOp salt which is important for the subsequent formation and isolation of the lanthanide complexes. The characteristic signature of the HtpOp formation is given by the ^{31}P NMR spectrum which shows a single peak at −10.5 ppm corresponding to the equivalent phosphorus atoms (Figure S1). The absence of a peak at −16.5 ppm indicates the absence of any triphenyl phosphate starting material. The shift corresponds well with the reported isolated acidic form.[23,24] Interestingly, the phosphorus signal observed for HtpOp is shifted to a lower frequency by 47 ppm in comparison to that of Htpip, indicating that, as expected, the phosphorus bears more electron density in the presence of the phenoxide groups. The powder IR spectrum shows bands at 2,961 cm^{-1} due to the N−H stretching vibrations. The P O stretching frequency is centered at 1184 cm^{-1} and a sharp absorption band at 933 cm^{-1} is due to PNP stretching frequencies. The ^{31}P NMR resonance shifts to −7.2 ppm in KtpOp as expected for the deprotonated form (Figure S2).

Crystals of KtpOp were grown from slow evaporation from aqueous solution at room temperature and the crystallographic information is given in Table S1. The structure contains two independent formula units (Figure 1). Each potassium ion is coordinated by six oxygen atoms with distances in the range 2.634(3) Å to 2.880(4) Å. The P−N bond distances are in the range of 1.553(4)−1.560(4) Å and are shorter in comparison to those observed for HtpOp (1.64 Å).[13] The observed P−O distances of 1.472(3), 1.479(3), 1.479(3), and 1.469(3) Å for P(1)−O(3), P(2)−O(6), P(3)−O(9), and P(4)−O(12), respectively, are slightly greater than the P−O bond lengths of 1.46 Å in the free ligand. This is indicative of delocalization of π-electrons around the binding unit. The aromatic moieties of the ligand are involved in intramolecular interactions. Edge-to-face interactions are observed for pairs of phenoxide rings

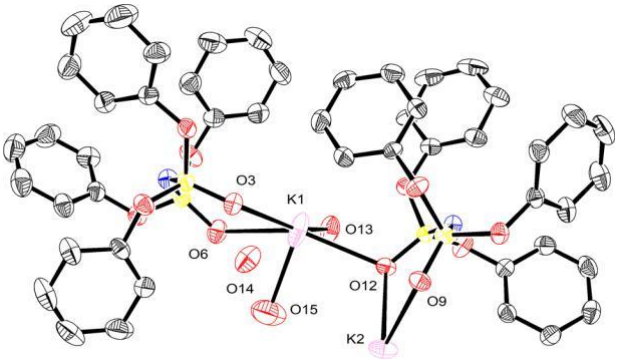

Figure 1. Asymmetric unit of the crystal structure of KtpOp with numbering scheme. Hydrogen atoms and one component of the disordered molecule are omitted for clarity.

with centroid-to-centroid distances of 4.93−5.40 Å. There is also evidence of a weak π−π stacking in one ligand, as two rings are almost parallel and have a centroid-to centroid separation of 4.14 Å. Both P−O and P−N bonds in KtpOp are significantly shorter than those reported for KMetpip.[7]

Synthesis and Characterization of Ln(tpOp)$_3$ Complexes. Reaction of $LnCl_3 \cdot 6H_2O$ with KtpOp in a 1:3 ratio gives the corresponding Ln(tpOp)$_3$ complexes as white powders with yields of 52−67%. The complexes have good solubility in chloroform, acetone, acetonitrile, methanol, and THF. Crystals for X-ray analysis were obtained by slow evaporation of the isolated powder from chloroform (Eu and Dy) or acetonitrile (Tb, Gd, and Er) solution and the crystallographic information are summarized in Table S2. The Ln(tpOp)$_3$(EtOH) (Ln = Tb, Eu, Dy, Gd, and Er) complexes all possess similar triclinic structures in the $P\bar{1}$space group, with lanthanide ions being seven-coordinated by three tpOp ligands and one additional ethanol molecule, resulting in a capped octahedral geometry. The crystal structure of Tb-(tpOp)$_3$ is shown as a representative example (Figure 2) with

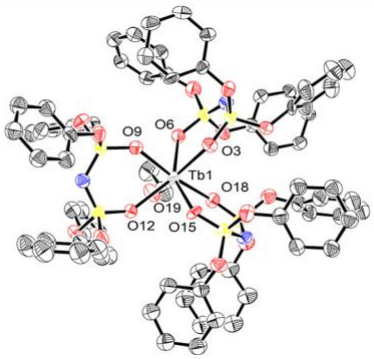

Figure 2. X-ray crystal structure of Tb(tpOp)$_3$(EtOH) with numbering scheme. Hydrogen atoms and one component of the disordered molecule are omitted for clarity.

the rest of the structures included in Figure S4. The bond distances between Tb and oxygen atoms from tpOp vary in the range of 2.27(1)−2.45(2) Å. The ethanol molecule is directly coordinated to the Tb^{3+} ion via O(19) atom, with a Tb(1)−O(19) distance at 2.403(6) Å. The average distances of P−O (O coordinated to Tb) and P−N bonds are 1.481 and 1.565 Å, respectively. It is interesting to note that the difference of the bond lengths between P−O and P−N bonds is larger in

$Tb(tpOp)_3$ than $Tb(tpip)_3$ which indicates that the electron density in the imidodiphosphonate binding unit is not as equally distributed as in the imidodiphosphinate unit.[7,8] The distance between the Tb ion and the furthest carbon atom (range 6.887−8.647 Å) is longer in $Tb(tpOp)_3$ than that observed for $Tb(tpip)_3$ (range 6.301−7.333 Å) suggesting a more extended "shell" around the lanthanide ion. The average acute O−Tb−O angle is 80.49°. Edge-to-face interaction between aromatic rings and π−π stacking is observed from the packing of the structure (Figure S5), where the shortest intermolecular Ln−Ln distance is found to be 9.920 Å and the next longest is 13.534 Å.

The crystal structure of $Yb(tpOp)_3$ was previously described by Kulpe[16,17] where the Yb^{3+} ion is coordinated by three tpOp ligands with no solvent molecules associated with the coordination sphere of the ytterbium ion. The absence of ethanol in $Yb(tpOp)_3$ is probably due to the smaller Yb^{3+} ionic radius.

The average Ln−O bond lengths decrease in the following order Eu > Gd > Tb > Dy > Er > Yb which is expected due to the stronger interaction of the smaller lanthanides. All the lanthanide complexes are involved in intramolecular interactions including π−π stacking and the edge-on association between C−H and phenoxide rings, which play an important role in stabilizing the hydrophobic shell formed by the twelve phenoxide groups around the central lanthanide.

To evaluate the effect of the shell around the lanthanide, we calculate the normalized ligand shielding. This is the percentage of the metal coordination sphere shielded by a ligand L for the metal−L distance of 2.28 Å (calculated individually for each ligand). The values for the sum for all ligands are 85% for $Tb(tpOp)_3$, $Gd(tpOp)_3$, $Dy(tpOp)_3$, $Er(tpOp)_3$ and 103% for $Yb(tpOp)_3$ and $Eu(tpOp)_3$. The values excluding the coordinated EtOH are 72% for $Tb(tpOp)_3$, $Er(tpOp)_3$, $Gd(tpOp)_3$, $Dy(tpOp)_3$, 103% for $Yb(tpOp)_3$ and 90% for $Eu(tpOp)_3$ These values indicate the ligand occupation around the lanthanide coordination sphere.

The lanthanide complexes display characteristic ^{31}P chemical shifts summarized in Table S3. All complexes display a single resonance, indicating the presence of one phosphorus environment and confirm the equivalence of the ligands. In the yttrium complex, $Y(tpOp)_3$, which is examined as a diamagnetic analogue, the ^{31}P resonance moves from δ = −9.7 of the HtpOp to −4.2 ppm as expected due to the coordination of the lanthanide triply charged cation. The $Ln(tpOp)_3$ complexes can be separated into three groups by the signs of the ^{31}P chemical shifts with respect to the difference with the diamagnetic complex $Y(tpOp)_3$. The shifts of Dy^{3+}, Sm^{3+}, and Yb^{3+} complexes remain similar to that of the $Y(tpOp)_3$ complex, whereas the Er^{3+}, Eu^{3+}, and Tb^{3+} complexes show the greatest upfield ^{31}P shifts, while Nd^{3+} complex has the largest downfield field. The observed changes arise from the effect of the paramagnetic lanthanide. Two types of interaction between the lanthanide and the ligand can influence the shifts: the contact and pseudocontact interactions. The shifts across the series for $Ln(tpOp)_3$ do not follow the predicted trends, neither pseudocontact nor contact-only interactions predominate, and there is rather a contribution of both interactions. However, in the case of $Ln(tpip)_3$ complexes the ^{31}P shifts followed the contact only trend and in the case of the fluorinated complexes $Ln(F_{20}tpip)_3$ the shifts followed the pseudocontact trend. Clearly the electron-donating property of the ligand is important for the shifts. The shorter P−O bonds observed for the $Ln(tpOp)_3$ in comparison with the $Ln(tpip)_3$ also support the difference of the environment around the phosphorus.

Steady-State Emission Studies of $Ln(tpOp)_3$. The complexes absorb light in the ultraviolet region, attributed to the HtpOp ligand. The absorption spectrum of $Tb(tpOp)_3$ (Figure 3) exhibits an intense structured band with λ_{max} at 262 nm and two weaker bands at 257 and 270 nm, which can be assigned to the π → π* transitions of phenoxide aromatic groups, while the shoulder band at 300 nm can be identified as the n → π* transition of free ligand. The excitation spectrum of $Tb(tpOp)_3$ monitoring the $^5D_0 \rightarrow {}^7F_3$ transition at 620 nm shows that efficient energy transfer is observed from tpOp ligand to the lanthanide center (Figures 3 and S6). Interestingly the 300 nm band appears stronger in the excitation spectra of $Eu(tpOp)_3$ and $Tb(tpOp)_3$ than that in the spectra of $Dy(tpOp)_3$ which suggests that efficient energy transfer is taking place for those complexes from a lower state than in the case of $Dy(tpOp)_3$ (Figure S7).

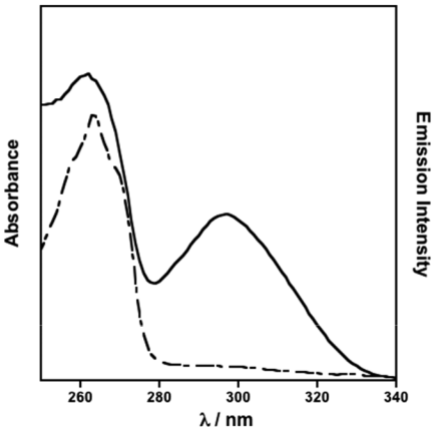

Figure 3. UV−vis (dashed line) and corrected excitation (solid line) spectra (λ_{em} = 620 nm) of $Tb(tpOp)_3$ in dry acetonitrile (5×10^{-5} M).

Upon excitation at 290 nm, characteristic emission in the visible was observed for Eu^{3+}, Tb^{3+}, Dy^{3+}, and Sm^{3+} complexes in solution and solid state (Figures 4 and S8). The complexes also show the characteristic emission under 270 nm excitation and a range of lower concentrations from 10^{-5} to 10^{-4} M. For $Eu(tpOp)_3$, the observed bands at 577, 589, 612, 651, and 700

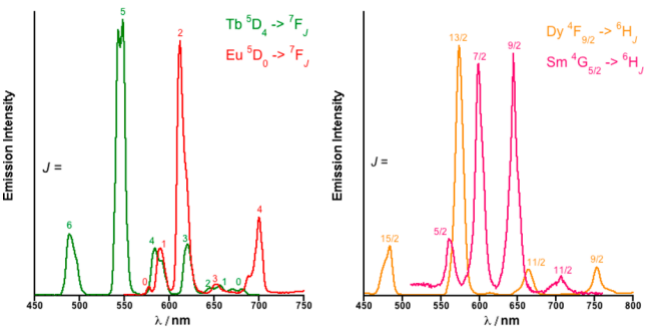

Figure 4. Emission spectra of $Eu(tpOp)_3$ (red, 0.18 mM), $Tb(tpOp)_3$ (green, 0.17 mM), $Dy(tpOp)_3$ (yellow, 0.63 mM), and $Sm(tpOp)_3$ (pink, 0.18 mM) in dry acetonitrile (λ_{exc} = 290 nm).

nm are attributed to the transitions of $^5D_0 \rightarrow {}^7F_J$ (J = 0, 1, 2, 3, and 4). In Tb(tpOp)$_3$, the observed bands at 488, 549, 583, 620, 644, 655, and 680 nm are attributed to the $^5D_4 \rightarrow {}^7F_J$ (J = 6, 5, 4, 3, 2, 1, and 0) transitions. In the solid state, the emission bands attributed to the hypersensitive transitions show characteristic splitting. The $^5D_0 \rightarrow {}^7F_2$ in Eu(tpOp)$_3$ splits at 612 and 620 nm, and the $^5D_4 \rightarrow {}^7F_5$ transition in Tb(tpOp)$_3$ splits at 541 and 548 nm (Figure S8). The splitting of these bands is due to their sensitivity to the symmetry of the coordination environment, and it is in agreement with the distorted symmetry of the oxygen donor atoms around Eu^{3+} ion observed in the crystal structure. Excitation of Dy(tpOp)$_3$ and Sm(tpOp)$_3$ in solution at 290 nm leads to the characteristic yellow and pink emission of Dy^{3+} and Sm^{3+}. The observed bands at 483, 572, 663, and 751 nm are assigned to $^4F_{9/2} \rightarrow {}^6H_J$ (J = 15/2, 13/2, 11/2, and 9/2) transitions for Dy^{3+}, and the bands at 561, 599, 644, and 705 nm for Sm^{3+} are assigned to $^4G_{5/2} \rightarrow {}^6H_J$ (J = 5/2, 7/2, 9/2, and 11/2) transitions, respectively.

To investigate the formation of the complexes in solution, a solution of KtpOp was titrated into $TbCl_3 \cdot 6H_2O$ in methanol (Figure S9). The emission intensity of Tb^{3+} increased until it reached a plateau with no further increase after 3 equiv of KtpOp. This confirms the formation of the complex with in situ mixing of the lanthanide and the ligand.

In order to determine the triplet state energy of the ligand, the emission properties of the Gd(tpOp)$_3$ were examined (Figure 5). Gadolinium has high-energy states, which do not

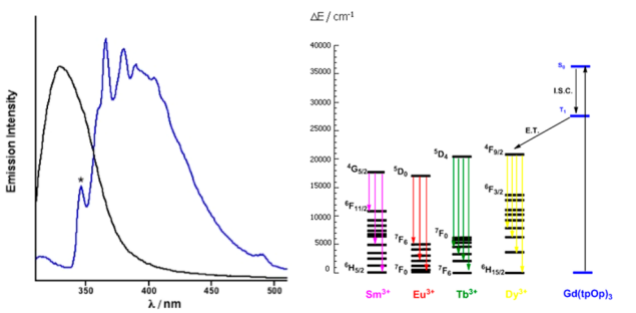

Figure 5. Room-temperature (black) and 77 K emission (blue) of Gd(tpOp)$_3$ in MeOH/EtOH 1:4 solution (3.1×10^{-5} M), λ_{exc} = 290 nm. Schematic energy level diagram to show intersystem crossing (ISC) and the energy transfer (ET) process.

interfere with the ligand triplet state but will still influence intersystem crossing to increase the prevalence of the triplet state of the ligand by the heavy atom effect. The room-temperature emission spectrum of Gd(tpOp)$_3$ in MeOH/ EtOH (1:4) displays a broad band centered at 330 nm, which corresponds to the fluorescence originating from the tpOp ligand. Upon cooling to 77 K, the ligand phosphorescence is clearly observed, and the band exhibits a characteristic fine structure based on the vibronic transitions. The energy of the progressive vibronic transitions was calculated (Table S4) and the $^3\pi-\pi^*$ state of the ligand was evaluated to be 27 397 cm^{-1} from the 0−0 transition spectrum at 77 K. The triplet level energy is consistent with energy observed experimentally for phenol (28 089 cm^{-1}) in water.[25]

The photophysical properties leading to efficient energy transfer are related to the energy gap between singlet and triplet excited states of the ligand for an efficient intersystem crossing process. Previous publications indicate that the intersystem crossing process is efficient when $E(^1\pi\pi^*)$ to $(^3\pi\pi^*)$ is at least 5000 cm^{-1}.[26,27] The singlet energy state of the absorbing ligand was estimated at 34 483 cm^{-1}, from the absorbance edge of the Gd(tpOp)$_3$ complex which leads to an energy gap between the $^1\pi\pi^*$ and $^3\pi\pi^*$ level of 7086 cm^{-1}, indicating a sufficient gap for intersystem crossing in Ln(tpOp)$_3$ complexes. The energy of the ligand triplet level relative to the lanthanide lower excited state is important for efficient energy transfer from the ligand triplet to the lanthanide excited state. The emitting levels of Tb^{3+} ($^5D_4$, 20 500 cm^{-1}), Eu^{3+} ($^5D_0$, 17 200 cm^{-1}), Dy^{3+} ($^4F_{9/2}$, 21 100 cm^{-1}), and Sm^{3+} ($^4G_{5/2}$; 17 700 cm^{-1})[28] lie well below the triplet state of ligand (27 397 cm^{-1}), and the energy gaps between ligand and metal-centered levels do not favor back energy transfer which can be observed at energy gaps of less than 3500 cm^{-1}.

The photophysical properties of NIR emitting complexes Nd(tpOp)$_3$, Er(tpOp)$_3$, and Yb(tpOp)$_3$ are studied in dry MeCN and solid state (Figures 6 and S10). At room-

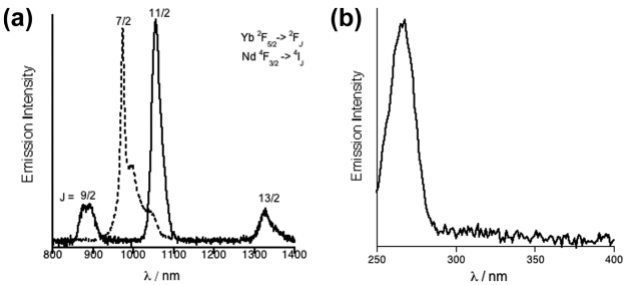

Figure 6. (a) Emission spectra of Yb(tpOp)$_3$ (dotted line, 0.42 mM) and Nd(tpOp)$_3$ (solid line, 0.56 mM) in dry acetonitrile (λ_{exc} = 290 nm) showing the $^2F_{5/2} \rightarrow {}^2F_{7/2}$ transition for Yb^{3+} and $^4F_{3/2} \rightarrow {}^4I_J$ (J = 9/2, 11/2, 13/2) for Nd^{3+}, respectively. (b) Corrected excitation spectrum of Yb(tpOp)$_3$ in dry acetonitrile (0.7×10^{-4} M λ_{em} = 974 nm).

temperature, sensitized emission is observed for Nd(tpOp)$_3$ and Yb(tpOp)$_3$ complexes. The Nd(tpOp)$_3$ emission displays three bands with peak maxima at 887, 1058, and 1328 nm which are assigned to the luminescent transitions of $^4F_{3/2} \rightarrow {}^4I_J$ (J = 9/2, 11/2, and 13/2), respectively. Excitation of Yb(tpOp)$_3$ at 290 nm leads to infrared emission with a sharp maximum at 974 nm and a broadened shoulder, corresponding to the $^2F_{5/2} \rightarrow {}^2F_{7/2}$ transition for Yb^{3+}. We found that the luminescence intensity is not enhanced upon deoxygenation of the samples, indicating that oxygen quenching of the triplet state of tpOp is not competing with the energy transfer to the lanthanide ion. The excitation spectrum of Yb(tpOp)$_3$ (Figure 6b) confirms the sensitization of the near-infrared lanthanide ion by the tpOp ligand. In the case of the Er(tpOp)$_3$ complex no emission was observed. This is possibly due to the large energy gap (20 000 cm^{-1}) between the triplet state energy level of tpOp (27 397 cm^{-1}) and the emitting level of Er^{3+} ($^4I_{13/2}$) at ~6,500 cm^{-1}, which results in nonradiationless quenching pathways taking place.

Time-Resolved Luminescence Studies of Ln(tpOp)$_3$.

The luminescence lifetimes of the Ln(tpOp)$_3$ complexes, following excitation into ligand-centered bands are summarized in Tables 1 and 2. All visible-light-emitting complexes show long lifetimes in solution which are slightly longer than the Ln(tpip)$_3$ analogues.

Table 1. Luminescence Lifetimes of $Ln(tpOp)_3$ in Dry CH_3CN[a]

complex	τ/ms
$Tb(tpOp)_3$	3.1
$Tb(tpOp)_3$ and 15% H_2O	2.0
$Eu(tpOp)_3$	2.7
$Eu(tpOp)_3$ and 15% H_2O	1.7[b]
$Dy(tpOp)_3$	0.20
$Sm(tpOp)_3$	0.20
$Tb(tpip)_3$	2.8
$Eu(tpip)_3$	1.8
$Dy(tpip)_3$	0.18
$Sm(tpip)_3$	0.15

[a]The effect of water addition and comparison with $Ln(tpip)_3$, detected for emissive levels Tb^{3+} ($^5D_4$), Eu^{3+} ($^5D_0$), Dy^{3+} ($^4F_{9/2}$), and Sm^{3+} ($^4G_{5/2}$). λ_{exc} = 290 nm. Values are reproducible to ±5%. [b]This sample displayed a biexponential lifetime with a major (93%) long component of 1.7 ms and a short component of 0.6 ms (7%).

Table 2. Luminescence Lifetimes of Near-Infrared Emissive $Ln(tpOp)_3$ in Dry CH_3CN[a]

complex	τ/μs
$Nd(tpOp)_3$	3.3
$Yb(tpOp)_3$	20
$Nd(tpip)_3$	2.7
$Yb(tpip)_3$	53

[a]Detected at Nd^{3+} ($^4F_{3/2}$) and Yb^{3+} ($^2F_{5/2}$) emissive levels. λ_{exc} = 290 nm; values are reproducible to ±10%.

The variation of lifetimes observed for the different visible lanthanides can be explained by the energy gap E between the emissive state of the Ln^{3+} ion and the highest sublevel of its receiving ground state. The E for Dy^{3+} (7850 cm^{-1}) and Sm^{3+} (7400 cm^{-1}) are very small, whereas for Tb^{3+} and Eu^{3+} the gaps are considerably larger at 14 800 and 12 300 cm^{-1}, respectively; therefore, only the high-energy O−H oscillators contribute to vibrational quenching.[29] The smaller gap for Dy^{3+} and Sm^{3+} results in lower frequency vibrations causing significant deactivation, hence the shorter values of the lifetimes.

To examine the number of inner-sphere water molecules, q, we used an established approach based on the luminescence lifetimes of the complexes upon addition of water (Table 1).[30,31] We obtained q = 0.7 ± 0.5 and 0.3 ± 0.5 for $Tb(tpOp)_3$ and $Eu(tpOp)_3$ respectively, in CH_3CN with addition of 15% water.

We also used modifications of the equation to reflect the outer-sphere effects of water using reported correction factors[1,32,33] adapted for acetonitrile solution:[31]

$$q' = A\,(k_{H_2O} - k_{CH_3CN} - B) \quad (1)$$

where A and B are parameters for inner- and outer-sphere water contributions to the luminescence quenching (see the Supporting Information for further details). The values for the complexes are calculated as q′ = 0.6 ± 0.5 and 0 ± 0.5 for the $Tb(tpOp)_3$ and $Eu(tpOp)_3$, respectively.

The calculated values give an average of water molecule occupation in the coordination spheres and within error they suggest that most of the molecules bind to one water molecule to fill the coordination sphere. The same is expected for $Dy(tpOp)_3$ and $Sm(tpOp)_3$ complexes, since they have analogous coordination chemistry. The fact that there is space in the larger lanthanides for coordination of an additional molecule is also evidenced by the X-ray crystal structures of $Ln(tpOp)_3$ (Ln = Tb, Dy, and Eu) complexes, where an additional molecule of ethanol is coordinated to Ln^{3+} ions.

The near-infrared-emitting complexes show long luminescence lifetimes in nondeuterated solvents, comparable with those previously reported for the $Ln(tpip)_3$ complexes and lanthanide cryptate complexes in D_2O (Table 2).[34] The imidophosphonate ligand provides good protection of the lanthanide coordination sphere which is evident in the long luminescent lifetimes for all lanthanide complexes.

Overall, the long luminescence lifetimes observed may suggest the lack of deactivation pathways based on high energy vibrations or low-lying charge transfer bands. The latter is supported by the long luminescent lifetime results for $Eu(tpOp)_3$ and $Yb(tpOp)_3$ complexes for which the ligand to metal charge transfer bands are dominant radiationless quenching pathways as they are the easily reduced lanthanides.

Quantum Yield Studies of $Ln(tpOp)_3$. The overall efficiency of the sensitization process for $Ln(tpOp)_3$ (Ln = Tb, Dy, Eu, and Sm) was examined by measurements of the luminescence quantum yields (Table 3).

Table 3. Experimental Luminescence Quantum Yields for the Visible-Light-Emitting $Ln(tpOp)_3$ Complexes in Dry CH_3CN Solution (Ln = Tb, Eu, Dy, and Sm)[a]

complex	ϕ/%
$Tb(tpOp)_3$	45[b]
$Tb(tpip)_3$	20[8]
$Eu(tpOp)_3$	6.8[b]
$Eu(tpip)_3$	1.3[8]
$Dy(tpOp)_3$	0.40[b]
$Sm(tpOp)_3$	0.29[c]

[a]λ_{exc} = 290 nm. $Ln(tpip)_3$ (Ln = Tb and Eu) are shown as comparison. [b]Error is estimated at 5% relative to the quoted value. [c]Error is estimated at 10% relative to the quoted value.

The results show that HtpOp is a more efficient sensitizer than the Htpip ligand. Although the quantum yields of the $Dy(tpOp)_3$ and $Sm(tpOp)_3$ are still smaller than those of the other visible-emitting lanthanides, they are larger than all the other Htpip derivatives where the numbers were too small to be measured in some cases. The quantum yield of the $Dy(tpOp)_3$ is in a similar range to reported Dy^{3+} complexes based on chiral DOTA derivatives in water.[35] Both $Tb(tpOp)_3$ and $Eu(tpOp)_3$ show great improvement in quantum yield compared to those reported for $Tb(tpip)_3$ and $Eu(tpip)_3$ (20 and 1.3%).[8] In the case of the $Tb(tpOp)_3$, the high quantum yield is comparable to those reported for the cryptate-based complexes[36,37] and octadentate ligands in aqueous media.[38] This could be due to the efficient transfer between the lower lying energy state in the $Tb(tpOp)_3$ complex and the terbium emissive state.

The quantum yields of $Nd(tpOp)_3$ and $Yb(tpOp)_3$ in dry acetonitrile were both measured by integrating sphere and estimated from the observed luminescence lifetime. The quantum yield measurements using the integrating sphere gave results of 0.5% for $Nd(tpOp)_3$ and 1% for $Yb(tpOp)_3$. The estimation using the lifetime measurement which gives an

intrinsic quantum yield is based on (τ_{obs}) and the radiative lifetime values (τ_{rad}):[39]

$$\Phi_{Ln} = \tau_{obs}/\tau_{rad} \quad (2)$$

where estimated values of τ_{rad} in organic systems are 2000 and 800 μs for Yb^{3+} and Nd^{3+} ions, respectively. This latter method refers only to the lanthanide-based emission process and does not take into account the efficiency of intersystem crossing and energy transfer processes, giving the estimated quantum yield values (Φ_{Ln}) of 0.4% for $Nd(tpOp)_3$ and 1.0% for $Yb(tpOp)_3$ which compare well with the integrated sphere values and indicate an efficient energy transfer process.

The enhanced quantum yields in comparison to the Htpip complexes, especially for the visible emitting lanthanide complexes can be attributed to the lower gap of the triplet state of the HtpOp ligand with the lanthanide emitting state. The triplet state of the phenoxy group is about 1000 cm^{-1} lower than the benzyl substituent. Additionally, these can be attributed to the reduction of deactivation pathways from C− H high-energy vibration. The phenoxy group positions the C− H high-energy vibrations further away from the lanthanide in comparison to the Htpip as shown by the crystal structure. The latter affects especially Dy^{3+} , Nd^{3+}, and Yb^{3+} complexes where C−H vibrational oscillations have a great ability to efficiently quench f−f transitions.

CONCLUSION

Luminescent $Ln(tpOp)_3$ (Ln = Tb, Dy, Eu, Sm, Gd, Nd, Yb, and Er) complexes based on a tetraphenyl imidodiphosphonate ligand HtpOp have been synthesized and fully characterized. All complexes exhibit characteristic emission of Ln^{3+} ion in solution and powder samples at room temperature as well as relatively long-lived visible luminescence lifetimes. The long lifetimes and high quantum yields indicate that the HtpOp ligand positions the sensitizers far enough for the lack of radiationless deactivation pathways via high energy vibrations but close enough for efficient energy transfer. The latter is evident in the case of $Tb(tpOp)_3$ which exhibits high quantum yields. Even though the introduction of oxygen on the aromatic chromophores does not change the first coordination sphere of the Ln^{3+} ions, an impressive enhancement is still achieved in quantum yields. The observed results demonstrate that improvements in luminescence efficiency can be achieved by straightforward synthetic tuning of the ligand aromatic chromophores.

ASSOCIATED CONTENT

* Supporting Information

The Supporting Information is available free of charge on the ACS Publications website at DOI: 10.1021/acs.inorgchem.9b02090.

Additional NMR, absorption, emission and excitation spectra along with crystallographic data and structures (PDF)

Accession Codes

CCDC 1903281−1903286 contain the supplementary crystallographic data for this paper. These data can be obtained free of charge via www.ccdc.cam.ac.uk/data_request/cif, or by emailing data_request@ccdc.cam.ac.uk, or by contacting The Cambridge Crystallographic Data Centre, 12 Union Road, Cambridge CB2 1EZ, UK; fax: +44 1223 336033.

AUTHOR INFORMATION

Corresponding Author

*E-mail: z.pikramenou@bham.ac.uk.

ORCID

Benson M. Kariuki: 0000-0002-8658-3897

Yuan-Zhu Zhang: 0000-0002-1676-2427

Zoe Pikramenou: 0000-0002-6001-1380

Author Contributions

#D.D. and A.J.C. contributed equally to this work.

Notes

The authors declare no competing financial interest.

ACKNOWLEDGMENTS

We thank EPSRC, University of Birmingham, and Southern University of Science and Technology (SUSTech) for support.

REFERENCES

(1) Bünzli, J.-C. G. On the design of highly luminescent lanthanide complexes. Coord. Chem. Rev. 2015, 293−294, 19−47.

(2) Chow, C. Y.; Eliseeva, S. V.; Trivedi, E. R.; Nguyen, T. N.; Kampf, J. W.; Petoud, S.; Pecoraro, V. L. Ga3+/Ln3+ Metallacrowns: A Promising Family of Highly Luminescent Lanthanide Complexes That Covers Visible and Near-Infrared Domains. J. Am. Chem. Soc. 2016, 138, 5100−5109.

(3) Zhou, J.; Leaño, J. L., Jr.; Liu, Z.; Jin, D.; Wong, K.-L.; Liu, R.-S.; Bünzli, J.-C. G. Impact of Lanthanide Nanomaterials on Photonic Devices and Smart Applications. Small 2018, 14, 1801882.

(4) Ye, H. Q.; Li, Z.; Peng, Y.; Wang, C. C.; Li, T. Y.; Zheng, Y. X.; Sapelkin, A.; Adamopoulos, G.; Hernández, I.; Wyatt, P. B.; Gillin, W. P. Organo-erbium systems for optical amplification at telecommuni-cations wavelengths. Nat. Mater. 2014, 13, 382.

(5) Lu, H.; Peng, Y.; Ye, H.; Cui, X.; Hu, J.; Gu, H.; Khlobystov, A. N.; Green, M. A.; Blower, P. J.; Wyatt, P. B.; Gillin, W. P.; Hernández, I. Sensitization, energy transfer and infra-red emission decay modulation in Yb3+-doped NaYF4 nanoparticles with visible light through a perfluoroanthraquinone chromophore. Sci. Rep. 2017, 7, 5066.

(6) An, J.; Shade, C. M.; Chengelis-Czegan, D. A.; Petoud, S.; Rosi, N. L. Zinc-Adeninate Metal−Organic Framework for Aqueous Encapsulation and Sensitization of Near-infrared and Visible Emitting Lanthanide Cations. J. Am. Chem. Soc. 2011, 133, 1220−1223.

(7) Magennis, S. W.; Parsons, S.; Pikramenou, Z. Assembly of Hydrophobic Shells and Shields around Lanthanides. Chem. - Eur. J. 2002, 8, 5761−5771.

(8) Magennis, S. W.; Parsons, S.; Pikramenou, Z.; Corval, A.; Derek Woollins, J. Imidodiphosphinate ligands as antenna units in luminescent lanthanide complexes. Chem. Commun. 1999, 61−62.

(9) Bassett, A. P.; Van Deun, R.; Nockemann, P.; Glover, P. B.; Kariuki, B. M.; Van Hecke, K.; Van Meervelt, L.; Pikramenou, Z. Long-Lived Near-Infrared Luminescent Lanthanide Complexes of Imidodiphosphinate “Shell” Ligands. Inorg. Chem. 2005, 44, 6140− 6142.

(10) Glover, P. B.; Bassett, A. P.; Nockemann, P.; Kariuki, B. M.; Van Deun, R.; Pikramenou, Z. Fully Fluorinated Imidodiphosphinate Shells for Visible- and NIR-Emitting Lanthanides: Hitherto Unexpected Effects of Sensitizer Fluorination on Lanthanide Emission Properties. Chem. - Eur. J. 2007, 13, 6308−6320.

(11) Hu, J. X.; Karamshuk, S.; Gorbaciova, J.; Ye, H. Q.; Lu, H.; Zhang, Y. P.; Zheng, Y. X.; Liang, X.; Hernández, I.; Wyatt, P. B.; Gillin, W. P. High sensitization efficiency and energy transfer routes for population inversion at low pump intensity in Er organic complexes for IR amplification. Sci. Rep. 2018, 8, 3226.

(12) Nielsen, M. L. The Formation of P-N and P-N-P Bonds by Elimination of Phenol in a Basic Condensation. Inorg. Chem. 1964, 3, 1760−1767.

(13) Kulpe, S.; Seidel, I.; Herrmann, E. The structure of Tetraphenyl Imidodiphosphate, C24H21NO6P2. Cryst. Res. Technol. 1984, 19, 661−668.
(14) Nöth, H.; Fluck, E. Röntgenstrukturuntersuchungen an Verbindungen mit P NH P-Gerüst/X-Ray Structural Studies on Compounds with a P NH-P Backbone. Z. Naturforsch., B: J. Chem. Sci. 1984, 39, 744.
(15) Herrmann, E.; Nang, H. B.; Dreyer, R. Komplexe von Seltenerdelementen mit Imidodiphosphorsauretetraphenylester. Z. Chem. 1979, 19, 187−188.
(16) Kulpe, S.; Seidel, I.; Szulewsky, K.; Kretschmer, G. The structure of tris(tetraphenyl imidodiphosphato)ytterbium(III). Acta Crystallogr., Sect. B: Struct. Crystallogr. Cryst. Chem. 1982, 38, 2813− 2817.
(17) Kulpe, S.; Seidel, I.; Herrmann, E. Ein Seltenerdkomplex; Die Molekülstruktur des Tris(tetraimidodiphosphato)ytterbium(III), C72H60N3O18P6Yb. Z. Chem. 1981, 21, 333−335.
(18) Sheldrick, G. SHELXT - Integrated space-group and crystal-structure determination. Acta Crystallogr., Sect. A: Found. Adv. 2015, 71, 3−8.
(19) Guzei, I. A.; Wendt, M. An improved method for the computation of ligand steric effects based on solid angles. Dalton Trans. 2006, 3991−3999.
(20) Ishida, H.; Bünzli, J.-C.; Beeby, A. Guidelines for measurement of luminescence spectra and quantum yields of inorganic and organometallic compounds in solution and solid state. Pure Appl. Chem. 2016, 88, 701.
(21) Brouwer, A. M. Standards for photoluminescence quantum yield measurements in solution. Pure Appl. Chem. 2011, 83, 2213.
(22) Suzuki, K.; Kobayashi, A.; Kaneko, S.; Takehira, K.; Yoshihara, T.; Ishida, H.; Shiina, Y.; Oishi, S.; Tobita, S. Reevaluation of absolute luminescence quantum yields of standard solutions using a spectrometer with an integrating sphere and a back-thinned CCD detector. Phys. Chem. Chem. Phys. 2009, 11, 9850−9860.
(23) He, X.; Ji, Y.; Jin, Y.; Kan, S.; Xia, H.; Chen, J.; Liang, B.; Wu, H.; Guo, K.; Li, Z. Bifunctional imidodiphosphoric acid-catalyzed controlled/living ring-opening polymerization of trimethylene carbo-nate resulting block, α,ω-dihydroxy telechelic, and star-shaped polycarbonates. J. Polym. Sci., Part A: Polym. Chem. 2014, 52, 1009−1019.
(24) Kan, S.; Jin, Y.; He, X.; Chen, J.; Wu, H.; Ouyang, P.; Guo, K.; Li, Z. Imidodiphosphoric acid as a bifunctional catalyst for the controlled ring-opening polymerization of δ-valerolactone and ε-caprolactone. Polym. Chem. 2013, 4, 5432−5439.
(25) Mayer, G. V.; Bazyl', O. K.; Artyukhov, V. Y.; Sokolova, I. V. Electronically excited states of phenol and its water complexes and photoprocesses in them. Russ. Phys. J. 1999, 42, 431−435.
(26) Steemers, F. J.; Verboom, W.; Reinhoudt, D. N.; van der Tol, E. B.; Verhoeven, J. W. New Sensitizer-Modified Calix[4]arenes Enabling Near-UV Excitation of Complexed Luminescent Lanthanide Ions. J. Am. Chem. Soc. 1995, 117, 9408−9414.
(27) Klink, S. I.; Grave, L.; Reinhoudt, D. N.; van Veggel, F. C. J. M.; Werts, M. H. V.; Geurts, F. A. J.; Hofstraat, J. W. A Systematic Study of the Photophysical Processes in Polydentate Triphenylene-Functionalized Eu3+, Tb3+, Nd3+, Yb3+, and Er3+ Complexes. J. Phys. Chem. A 2000, 104, 5457−5468.
(28) Carnall, W. T.; Fields, P. R.; Rajnak, K. Spectral Intensities of the Trivalent Lanthanides and Actinides in Solution. II. Pm3+, Sm3+, Eu3+, Gd3+, Tb3+, Dy3+, and Ho3+. J. Chem. Phys. 1968, 49, 4412− 4423.
(29) Stein, G.; Würzberg, E. Energy gap law in the solvent isotope effect on radiationless transitions of rare earth ions. J. Chem. Phys. 1975, 62, 208−213.
(30) Horrocks, W. D.; Sudnick, D. R. Lanthanide ion probes of structure in biology. Laser-induced luminescence decay constants provide a direct measure of the number of metal-coordinated water molecules. J. Am. Chem. Soc. 1979, 101, 334−340.
(31) Renaud, F.; Piguet, C.; Bernardinelli, G.; Bünzli, J.-C. G.; Hopfgartner, G. Nine-Coordinate Lanthanide Podates with Predetermined Structural and Electronic Properties: Facial Organization of Unsymmetrical Tridentate Binding Units by a Protonated Covalent Tripod. J. Am. Chem. Soc. 1999, 121, 9326−9342.
(32) Dickins, R. S.; Gunnlaugsson, T.; Parker, D.; Peacock, R. D. Reversible anion binding in aqueous solution at a cationic heptacoordinate lanthanide centre: selective bicarbonate sensing by time-delayed luminescence. Chem. Commun. 1998, 1643−1644.
(33) Supkowski, R. M.; Horrocks, W. D. On the determination of the number of water molecules, q, coordinated to europium(III) ions in solution from luminescence decay lifetimes. Inorg. Chim. Acta 2002, 340, 44−48.
(34) Faulkner, S.; Beeby, A.; Carrie,́M.-C.; Dadabhoy, A.; Kenwright, A. M.; Sammes, P. G. Time-resolved near-IR lumines-cence from ytterbium and neodymium complexes of the Lehn cryptand. Inorg. Chem. Commun. 2001, 4, 187−190.
(35) Harris, M.; Vander Elst, L.; Laurent, S.; Parac-Vogt, T. N. Magnetofluorescent micelles incorporating DyIII−DOTA as potential bimodal agents for optical and high field magnetic resonance imaging. Dalton Trans. 2016, 45, 4791−4801.
(36) Alzakhem, N.; Bischof, C.; Seitz, M. Dependence of the Photophysical Properties on the Number of 2,2′-Bipyridine Units in a Series of Luminescent Europium and Terbium Cryptates. Inorg. Chem. 2012, 51, 9343−9349.
(37) Alpha, B.; Lehn, J.-M.; Mathis, G. Energy Transfer Luminescence of Europium(III) and Terbium(III) Cryptates of Macrobicyclic Polypyridine Ligands. Angew. Chem., Int. Ed. Engl. 1987, 26, 266−267.
(38) Law, G.-L.; Pham, T. A.; Xu, J.; Raymond, K. N. A Single Sensitizer for the Excitation of Visible and NIR Lanthanide Emitters in Water with High Quantum Yields. Angew. Chem., Int. Ed. 2012, 51, 2371−2374.
(39) Klink, S. I.; Hebbink, G. A.; Grave, L.; Peters, F. G. A.; Van Veggel, F. C. J. M.; Reinhoudt, D. N.; Hofstraat, J. W. Near-Infrared and Visible Luminescence from Terphenyl-Based Lanthanide(III) Complexes Bearing Amido and Sulfonamido Pendant Arms. Eur. J. Org. Chem. 2000, 2000, 1923−1931.